Materials Science & Engineering C 102 (2019) 764–772

Contents lists available at ScienceDirect

Materials Science & Engineering C

journal homepage: www.elsevier.com/locate/msec

Reduced graphene oxide decorated on Cu/CuO-Ag nanocomposite as a high-performance material for the construction of a non-enzymatic sensor: Application to the determination of carbaryl and fenamiphos pesticides

Pegah Hashemi[a], Nashmil Karimian[b], Hosein Khoshsafar[b], Fabiana Arduini[c], Mehdi Mesri[d], Abbas Afkhami[a], Hasan Bagheri[d,*]

[a] Faculty of Chemistry, Bu-Ali Sina University, Hamedan, Iran
[b] Research and Development Department, Farin Behbood Tashkhis LTD, Tehran, Iran
[c] Department of Chemical Science and Technologies, University of Rome Tor Vergata, Via della Ricerca Scientifica, 00133 Rome, Italy
[d] Chemical Injuries Research Center, Systems Biology and Poisonings Institute, Baqiyatallah University of Medical Sciences, Tehran, Iran

ARTICLE INFO

Keywords:
Reduced graphene oxide-Cu/CuO-Ag nanocomposite
Simultaneous determination
Pesticides
Modified electrodes
Electrochemical sensors

ABSTRACT

A novel electrochemical sensor based on the reduced graphene oxide-Cu/CuO-Ag nanocomposite modified glassy carbon electrode (rGO/Cu/CuO-Ag/GCE) has been applied for the simultaneous analysis of carbaryl and fenamiphos as two important pesticides. The electrochemical behavior of carbaryl and fenamiphos at rGO/Cu/CuO-Ag/GCE was studied by cyclic voltammetry and differential pulse voltammetry. The modified electrode exhibited two separated oxidation signals for the simultaneous determination of both carbaryl and fenamiphos with excellent sensitivity. The characteristics of the modified electrode were studied with transmission electron microscopy, X-ray diffraction and Fourier transform-infrared spectroscopy techniques. Under optimized conditions, the rGO/Cu/CuO-Ag/GCE detected carbaryl and fenamiphos with the wide linear ranges of 0.05–20 and 0.01–30 μM, and the detection limits were 0.005 and 0.003 μM, respectively. This developed electrochemical platform applied as a simple and cost-effective sensor for the detection of low levels of carbaryl and fenamiphos in fruit and vegetable samples successfully.

1. Introduction

In recent years, the rapid growth of population and industry as well as the need to increase food production allowed a large use of pesticides in agriculture, causing the contamination of natural water and foodstuff [1–3]. Carbaryl (CA) is one of the carbamic pesticides that act as insecticides which used on agricultural crops, home gardens, lawns, and other ornamental plants. Fenamiphos (FEN) is an organophosphorus insecticide (nematicide) that is used to control a wide variety of nematode (round worm) pests.

Hence, considering a large number of negative health and environmental effects of pesticides, determining of these pesticides is urgent to protect the environment and human health. Generally, gardeners and farmers, simultaneously use of pesticides in many cultures. Detection of CA and FEN was separately performed using chromatography methods such as high-performance liquid chromatography [4], gas chromatography [5], fluorimetry [6] and competitive immunoassays [7] that are usually time consuming, expensive and complicated. Besides these traditional methods, electrochemical techniques have attracted great popularity because simple, cost-effective, high efficiency and without the need of dedicated laboratories. To improve the performance of electrochemical sensors, various nanoparticles and carbon nanostructures were used to their modification [8,9]. Electrochemical biosensors based on the inhibition of target enzymes for the detection of pesticides have been widely developed in the past few years [10]. The application of enzymatic-based biosensors limited due to the intrinsic nature of enzymes that always require special care and have less stability. Also, these methods have great drawbacks while non-enzymatic electrodes are preferred due to good sensitivity and stability. Codognoto et al. reported the simultaneous detection of carbendazim and FEN by boron-doped diamond electrode [11]. Wang and coworkrs developed a new nonenzymatic sensor based on cobalt (II) oxide (CoO)-decorated reduced graphene oxide (rGO) for the determination simultaneous of carbofuran and CA in fruits and vegetables [12].

In recent years, rGO has attracted special consideration as an

* Corresponding author.
E-mail address: h.bagheri@bmsu.ac.ir (H. Bagheri).

https://doi.org/10.1016/j.msec.2019.05.010
Received 30 December 2018; Received in revised form 13 April 2019; Accepted 6 May 2019
Available online 07 May 2019
0928-4931/ © 2019 Elsevier B.V. All rights reserved.

intriguing nanomaterial which has the large surface area and high conductivity for electronic applications. The composites of rGO and the metallic nanoparticles (NPs) show the remarkable catalytic effect that were applied as the sensing platform in electrochemical sensors [13]. The bimetallic nanomaterials have better physicochemical properties such as high catalytic activity, functionality and stability in comparing to their individual metals [14]. Cu NPs had received particularly attractive to the synthesis of metallic nanostructures due to low cost, lower overpotential and facile production. In many studies, the noble metals were combined with Cu NP to form bimetallic NPs which enhance the catalytic properties and conductivity of nanocomposite. The bimetallic of Cu−Ni thin films were studied for the reduction of carbon dioxide [15], and also Pd−Cu NPs used as a good bimetallic catalyst in the Sonogashira reaction [16]. Furthermore, the metal oxides like SnO_2, CuO and TiO_2 decorated in the bimetallic are a kind of suitable materials to reduce the overpotentials for the electrochemical redox reactions that improved their catalytic properties. Among these metal oxides, CuO with a direct bandgap of 1.21–1.51 eV is known p-type semiconductors that distinguished properties make it suitable for the application for the gas sensors, photocatalyst and electrochemical sensors [17–21]. Sasmai et al. prepare a ternary composite of Cu_2O-Cu-CuO which showed higher catalytic activity than the metal Cu NPs for 4-nitrophenol reduction [22].

In this work, we synthesis the ternary Cu/CuO-Ag nanocomposite that consists of Ag and CuO NPs coexisted on the surface of metallic Cu NPs. Then, rGO decorated with Cu/CuO-Ag nanocomposite and applied as a modifier on the glassy carbon electrode (GCE) that exhibited superior catalytic activity toward oxidation of CA and FEN. To the best of our knowledge, there is not literature about the simultaneous electrochemical detection of CA and FEN. These pesticides are utilized continuously in various fields, so development a sensitive and stable sensor for the detection CA and FEN is worth of note. The prepared rGO/Cu/CuO-Ag/GCE displayed more sensitivity for the oxidation of CA and FEN than the Cu/CuO-Ag/GCE and Cu/CuO/GCE. The designed sensor exhibited excellent sensitivity and repeatability for determination of CA and FEN with a low detection limit.

2. Experimental

2.1. Reagents and apparatus

FEN and CA were provided from Sigma-Aldrich. Copper sulphate ($CuSO_4.5H_2O$), polyvinylpyrrolidone (PVP), hydrazine hydrate ($N_2H_4.H_2O$), cetyltrimethyl ammonium bromide (CTAB), and Silver nitrate ($AgNO_3$) were provided from Sigma-Aldrich. All other chemicals and reagents used in this work were of analytical grade and used as received without further purification. The stock solutions of the pesticides (1.0×10^{-3} M) were prepared in acetonitrile. The supporting electrolyte was a Britton-Robinson (B-R) buffer (0.1 M) changed from pH 1.0–10.0.

All electrochemical experiments were carried out by an Ivium potentiostat/galvanostat (Vertex, Ivium Technologies, and The Netherlands). The electrochemical cell consisted of the different modified electrodes as the working electrode; Ag/AgCl and platinum wire were applied as the reference and counter electrodes. All voltammetry measurements were performed at room temperature. The X-ray diffraction (XRD) spectra of the prepared samples were obtained by an X-ray powder diffractometer (38,066 Riva, d/G. *Via* M. Misone, 11/D (TN) Italy), using Kα radiation (λ = 1.5418 A°). FT-IR spectra were recorded in the range of 4000–500 cm^{-1} on a PerkinElmer, spectrum 100, FT-IR spectrometer and KBr pellet was used to prepare the samples for FT-IR measurements. The morphology and size of the nanoparticles were characterized by transmission electron microscopy (TEM, Philips, CM10, 100 KV).

2.2. Synthesis of Cu/CuO-Ag composite

Composite of Cu/CuO-Ag was synthesized by the method similar to that previously reported [23,24]. First, 6.25 g of $CuSO_4.5H_2O$ was dispersed in 100 mL ultrapure water and $NH_3.H_2O$ solution was added slowly into the solution that vigorously stirred. After the color of solution changed to clarify, 200 mg PVP and 200 mg CTAB added into 120 mL $[Cu(NH_3)_4]^{2+}$ solution under stirring. Finally, metallic Cu obtained from reduce $[Cu\ (NH_3)_4]^{2+}$ by added $N_2H_4.H_2O$ (10%,10 mL) into the mix solution. Then, the products after 6 h reaction were collected and washed several times with water and ethanol and finally dried under vacuum.

At second step, 200 mg of above product (Cu/CuO) was added into 50 mL ultrapure water and then adding $AgNO_3$ (0.05 M, 10 mL) aqueous solution dropwise to suspension under stirring to reduced Ag^+ for 6 h to complete the reaction. The resulting solid (Cu/CuO-Ag) was collected by centrifugation and after repeated washing was dried overnight in vacuum.

2.3. Preparation of rGO/Cu/CuO-Ag

0.06 g GO was synthesized by the modified Hummer's method [25] and then dispersed in 30 mL water and sonicated for 1 h. Thereafter the GO suspension was slowly added with Cu/CuO-Ag solution under sonication. After the suspension was stirred for 3 h, addition of 0.3 g urea and the mixture was stirred for another 3 h. The obtained product was dried at 200 °C for 1 h to remove the solvent and used for modification of the surface working electrode.

2.4. Preparation of the modified electrodes

The bare GCE was carefully polished with 3.0 and 0.05 μm alumina powders on the mirror like surface, then sonicated in ethanol and rinsed thoroughly with doubly distilled water. The modified electrode was prepared by dropping nanocomposite suspensions on the bare GCE surface.

The different solvents such as acetonitrile, ethanol, dimethylformamide (DMF), dichloroethane and nanocomposite amount deposited (from 2 to 20 μL of a solution 1 mg mL^{-1}) were also optimized. Finally, 6 μl of the rGO/Cu/CuO-Ag/DMF suspension was dropped on the clean GCE surface and then evaporating the solvent in air and finally was used as the working electrode. The GCEs modified with Cu/CuO-Ag and Cu/CuO was prepared by the same condition without the presence of rGO and rGO−Ag, respectively.

2.5. Sample preparation

To evaluate the performance of the sensor developed in real samples, the determination of CA and FEN in the fruit and vegetable samples such as grapes, oranges, tomatoes and cabbages were carried out by standard addition. The samples were exactly weighed and were cut into small pieces in the flask containing 30.0 mL ethanol. The mixture was sonicated for 50 min and then was centrifuged that the supernatant was collected for analysis. The different amounts of CA and FEN were spiked to obtain concentrations in the range linear of calibration curve.

3. Results and discussion

3.1. Characterization of rGO/Cu/CuO-Ag

The features and morphology of nanocomposites were characterized using TEM technique. Fig.1A exhibited the (a) graphene nanosheets and (b) Cu/CuO NPs that were irregular cuboids with the average size of 30 nm. A good deal of (c) Ag NPs were observed on the surface of Cu/CuO NPs without aggregation and finally Fig. 1A (d) rGO/Cu/CuO-Ag confirmed the presence of Cu/CuO, Ag, and rGO components in the

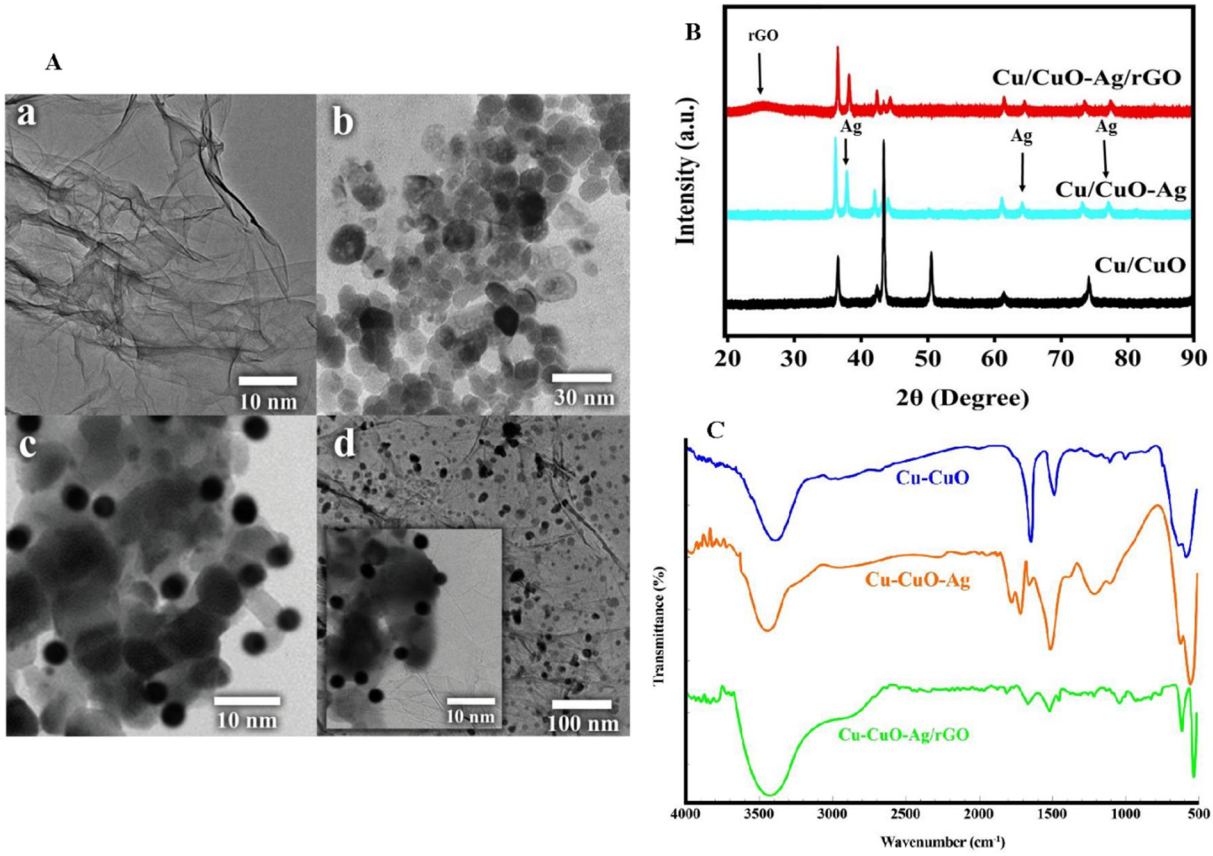

Fig. 1. A) TEM images of a) graphen, b) Cu/CuO, c) Cu/CuO-Ag and d) rGO/Cu/CuO-Ag nanocomposite; B) XRD patterns of Cu/CuO, Cu/CuO-Ag and rGO/Cu/CuO-Ag nanocomposite, C) FT-IR spectra of Cu/CuO, Cu/CuO-Ag and rGO/Cu/CuO-Ag nanocomposite.

synthesized composite. XRD was used as a rapid analytical technique for characterizing crystalline materials. XRD patterns of Cu/CuO, Cu/CuO-Ag and Cu/CuO-Ag/rGO composites were presented in Fig.1B. According to XRD patterns, Cu/CuO NPs have five diffraction peaks observed at 38°, 43°, 50°, 58° and 75° that indicating the presence of Cu and CuO without any other impurities [23]. In the spectrums of Cu/CuO-Ag nanocomposite, the presence of Ag in the composition was showed with three peaks that show in the Fig.1B. Also, the broad peak of graphene at 23° was observed in the spectrum of Cu/CuO-Ag/rGO composite which have been reported [26]. The FT-IR transmission spectra (Fig. 1C) of nanocomposites displayed the peaks in 3400 and 1630 cm^{-1} may be assigned to O—H stretching and binding vibrations. Moreover, the peaks appeared at 1050 cm^{-1} (C—O), 1650 cm^{-1} (C=C), 1400 cm^{-1} (C-OH) and 2950 cm^{-1} (C—H) are attributed to reduced graphene oxaide. Also, observed peaks at around 500 cm^{-1} are attributed to metallic oxide bond, which proves the formation of metallic nanocomposite in the presence of the rGO.

3.2. Electrochemical impedance spectroscopy

Electrochemical impedance spectroscopy (EIS) was used as efficient technique to characterize charge transfer process on the surface of the electrodes [27,28]. The examination is usually performed with redox-probe ferrocyanide/ferricyanide that the semicircle portion of the EIS represented the charge electron-transfer resistance (Rct) at the electrode surface. Fig. 2A shows the Nyquist plots of modified electrodes in the presence of 0.1 M KCl solution containing 5.0 mM $[Fe(CN)_6]^{3-/4-}$. As can be seen, bare GCE displays a semicircle with R_{ct} about 2.46 kΩ (curve a). The charge transfer was reduced to curve b after modification of GCE with Cu/CuO composite (R_{ct} = 1.28 kΩ) while the value of R_{ct} of Cu/CuO-Ag/GCE was very small (R_{ct} = 675 Ω). Once rGO added to Cu/CuO-Ag composite (curve c), the semicircle was smaller than others (386 Ω, curve d) because conductivity of the electrode increased and facilitated the arrival of the $K_3Fe(CN)_6$ at the electrode surface as well.

The CVs in 0.1 M KCl containing 5.0 mM $[Fe(CN)_6]^{3-/4-}$ were used for investigation of the electrochemical properties and peak to peak separation values of the bare GCE, Cu/CuO/GCE, Cu/CuO-Ag/GCE and rGO/Cu/CuO-Ag/GCE. As shown in the Fig. 2B, a standard redox peak could be seen (curve a) for bare GCE. The peak current was increased after the modification of the GCE with Cu/CuO and Cu/CuO-Ag (curve b, c) and this indicated its larger effective surface areas and enhanced the electron transfer on the electrodes surface. However, the redox peaks at the rGO/Cu/CuO-Ag/GCE show the highest peak currents in comparison to other electrodes. This increase in sensitivity and active electrode surface area contributed to the coating of rGO on Cu/CuO-Ag/GCE.

Moreover, the effect of potential scan rate was examined on the responses of rGO/Cu/CuO-Ag/GCE in the probe at scan rates higher than 200 mV s^{-1} that peak separations (ΔEp) increased due to charge transfer kinetics. By plotting the variation of the peak potential *versus* the logarithm of the scan rate (Fig. 2C) based on the Laviron theory (Eq. (1)) determined the charge transfer coefficient (α) and heterogeneous electron transfer rate constant (ks) [29].

$$E_{pc} = E^{0,} - \left[\frac{2.3RT}{\alpha nF}\right]\log\left\{\left[\frac{\alpha nF}{RT}\right]\times\left[\frac{\upsilon}{Ks}\right]\right. \quad (1)$$

According to slope (S) and intercept of Eq. (1) are:

$S = -\frac{2.3RT}{\alpha nF.}$

Intercept $= E^{0,} + S\log\frac{-2.3}{S} - Slog(Ks)$

the transfer coefficient (α) was calculated from the slope and found to be 0.41. The heterogeneous electron transfer rate constant (K_s) was obtained by introducing values of α and $E^{0'}$ in the Eq of intercept that

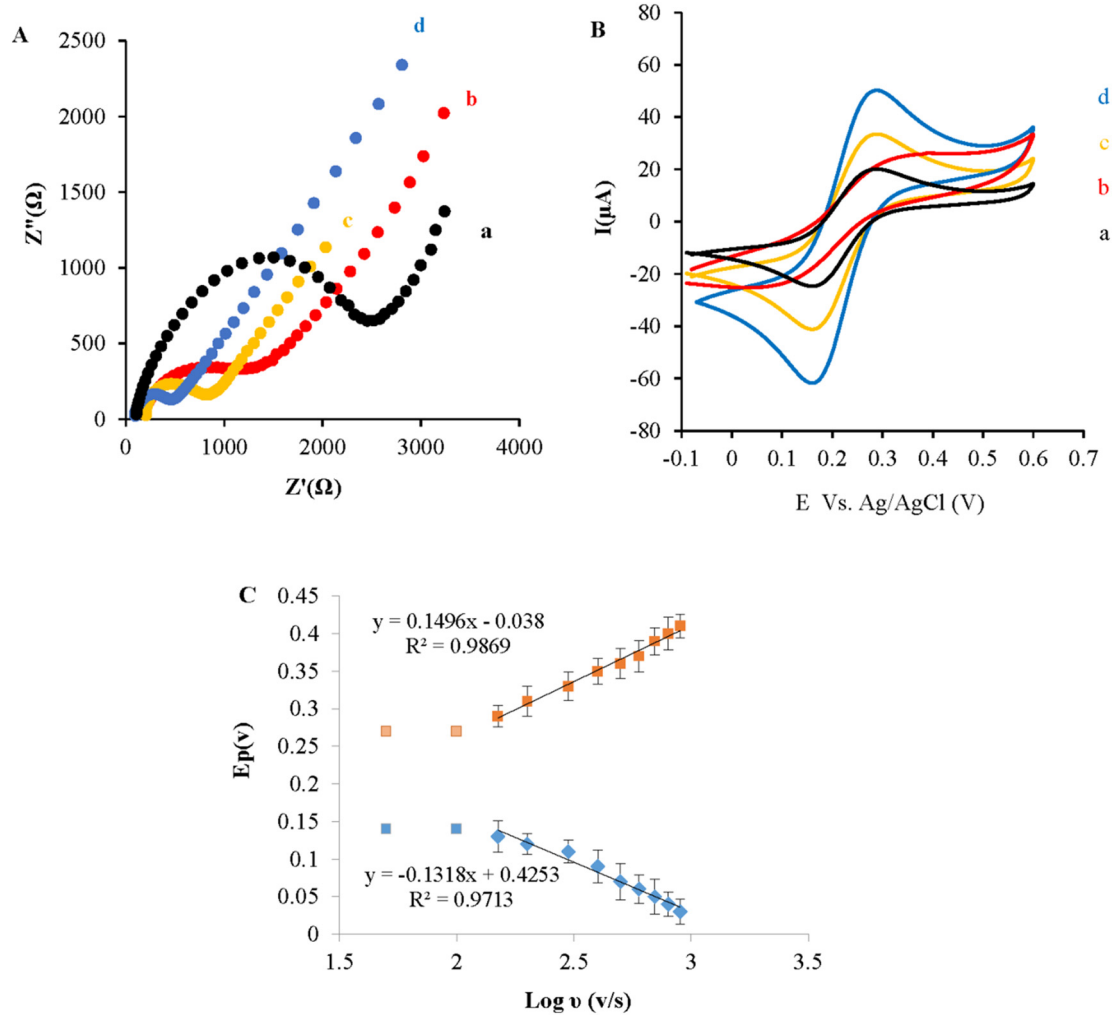

Fig. 2. A) EIS of 0.1 M KCl containing 5.0 mM $Fe(CN)_6^{3-/4-}$ at (a) bare GCE; (b) Cu/CuO/GCE (c) Cu/CuO-Ag/GCE, (d) rGO/Cu/CuO-Ag/GCE.
B) CVs of 0.1 M KCl containing 5.0 mM $Fe(CN)_6^{3-/4-}$ at (a) bare GCE; (b) Cu/CuO/GCE (c) Cu/CuO-Ag/GCE, (d) rGO/Cu/CuO-Ag/GCE.
C) Plot of peak potentials of rGO/Cu/CuO-Ag GCE in 0.1 M KCl containing 5.0 mM $Fe(CN)_6^{3-/4-}$ *vs.* logarithm of the scan rate from 50 to 900 mv/s.

found to be 2.59 s^{-1}. The results prove the fast electron transfer rates of the compounds on the designed sensor surface

3.3. Electrochemical behavior of CA and FEN at rGO/Cu/CuO-Ag/GCE

In order to investigate the electrochemical behavior of the modified electrodes, CV and DPV were used in the 0.1 M B-R buffer (pH = 3.0) containing 1.0 μM CA and 1.0 μM FEN. As shown in Fig. 3A, the CVs exhibited two oxidation peaks of CA and FEN at 1.04 and 1.35 V *vs.* Ag/AgCl without any cathode peak on the surface of different electrodes [11,30]. The oxidation peaks of CA and FEN on the bare GCE were poor and indistinct that indicated the electron transfer rates are slow at the electrode surface. However, the current responses of CA and FEN at the Cu/CuO/GCE and Cu/CuO-Ag/GCE are much higher than the bare GCE and the peak potentials somewhat shifted to less positive. They have attributed to the large active surface area of the modified electrodes and synergistic effect from Cu and Ag to increase catalytic activity in compare to the bare GCE. Combination of Cu/CuO and Ag nanoparticles developed a new composite for the modified electrodes by incorporate the features of Cu and CuO with Ag nanoparticles. The increased peak currents intensity can be due to the composite of Cu/CuO-Ag that exhibited surprisingly higher catalytic activity than that of the metal Cu NPs or Ag Nps individually [22]. Also, the unique characterization of rGO can be improved conductivity, when rGO is added to the Cu/CuO-Ag composition. The maximum response is observed for rGO/Cu/CuO-Ag/GCE due to facilitated electron transfer at the electrode surface.

Moreover, DPV of CA and FEN on the various electrodes in the B-R buffer (pH = 3) shown in Fig. 3B. The bare GCE showed two very small and broad peaks toward CA and FEN. The comparison of oxidation peak currents of CA and FEN at the Cu/CuO/GCE, Cu/CuO-Ag/GCE and rGO/Cu/CuO-Ag/GCE indicate that the current responses are well increased and separated for the three modified electrode while the maximum peak currents for CA and FEN were observed in the surface rGO/Cu/CuO-Ag/GCE. Therefore, rGO/Cu/CuO-Ag composite is suitable as a sensing layer for the simultaneous detection of CA and FEN in their mixture.

3.4. Effect of pH on the oxidation of CA and FEN

The influence of supporting electrolytes and pH was investigated using DPV on the peak potentials and peak currents in the pH range of 1.0–9.0. The response of rGO/Cu/CuO-Ag/GCE for CA (1.0 μM) and FEN (1.0 μM) were compared in the different supporting electrolytes such as HCl, HNO_3, acetate, borate and B-R buffers. The maximum response was obtained with 0.1 M B-R buffer and so, it was chosen the subsequent experiments.

The response of rGO/Cu/CuO-Ag/GCE were investigated in 0.1 M B-R buffer in the different pHs (pH 1.0–9.0) containing of 1.0 μM CA and 1.0 μM FEN. As shown in inset of Fig. 4A, the highest peak currents for

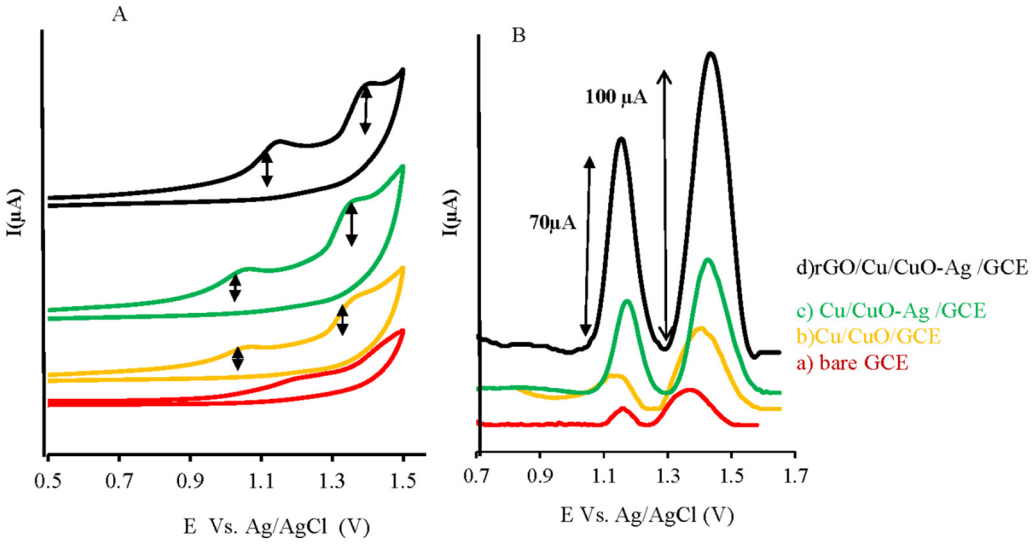

Fig. 3. (A) CVs and (B) DPVs in the presence of 1.0 μM CA and 1.0 μM FEN in the B-R buffer solution (pH = 3.0) on the surface of bare GCE and modified electrodes, Scan Rate = 100 mV s^{-1}.

both CA and FEN were obtained at pH = 3.0 and then decreases gradually. So, pH 3.0 is selected as the optimal pH value in the electrochemical measurements. The variation of oxidation peak potentials (E_{pa}) of CA and FEN with pH were studied (Fig. 4B). It can be seen that the E_{pa} linearly shift toward less positive values with the increase of pH and two regression equations of E_{pa} (CA) = −0.0572 pH + 1.3358 (R^2 = 0.9923), E_{pa} (FEN) = −0.0473 pH + 1.5144 (R^2 = 0.9758) were obtained.

The slopes of E_{pa} *vs.* pH plot for CA and FEN are near the theoretical value of −0.059 V/pH at 25 °C that indicated the number of protons and electrons are equal in the oxidation processes of CA and FEN, as observed in the literatures [11,12,30–32].

3.5. Effects of scan rate

The influence of scan rate on the oxidation peak currents of CA and FEN at rGO/Cu/CuO-Ag/GCE were investigated for study the nature of the electrode reaction. Fig. 5 showed the oxidation peak currents of cyclic voltamograms increase when the scan rate increase from 10 to 500 mVs^{-1}. A good linearity was obtained between the peak currents and the square root of scan rates ($v^{1/2}$), indicating the oxidation of both pesticides were a diffusion-controlled process. The linear equations of CA and FEN are expressed as follows:

$I_p(CA) = 1.9263\ v^{1/2} - 3.9244\ R^2 = 0.9891$

$I_p(FEN) = 2.0917\ v^{1/2} + 2.1131\ R^2 = 0.9921$

Also, a linear relationship between the logarithm of peak current (log I_{pa}) and logarithm of the scan rates (log v) was obtained that linear regression equations of CA and FEN as log I_p = 0.605 log v − 0.0381 (R^2 = 0.995) and log I_p = 0.4649 log v + 0.4368 (R^2 = 0.994), respectively. According to the above equations, the slope values are closed to theoretical value of 0.5 that confirmed oxidations of these pesticides on designed sensor are diffusion-controlled processes.

3.6. Individual and simultaneous detection of CA and FEN

The change of oxidation peaks currents with the increasing concentration of CA and FEN were separately and simultaneously investigated by the DPV technique under optimum conditions. The individual determination were performed for CA and FEN at rGO/Cu/CuO-Ag/GCE in B-R buffer solution (pH = 3.0) while the concentration of one pesticides was varied and the other pesticide concentration was constant. Fig. 6A shows the peak currents of CA increased with its rising

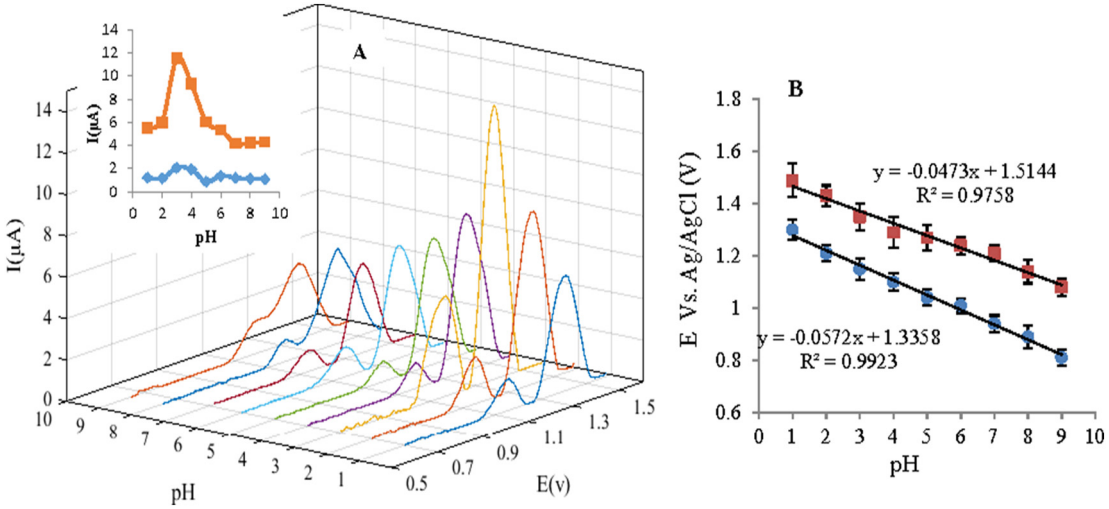

Fig. 4. A) DPVs of B-R buffer solution containing 1.0 μM CA and 1.0 μM FEN in the different pH (1–9), B) Plot of the anodic peaks potential *vs.* pH of the solution.

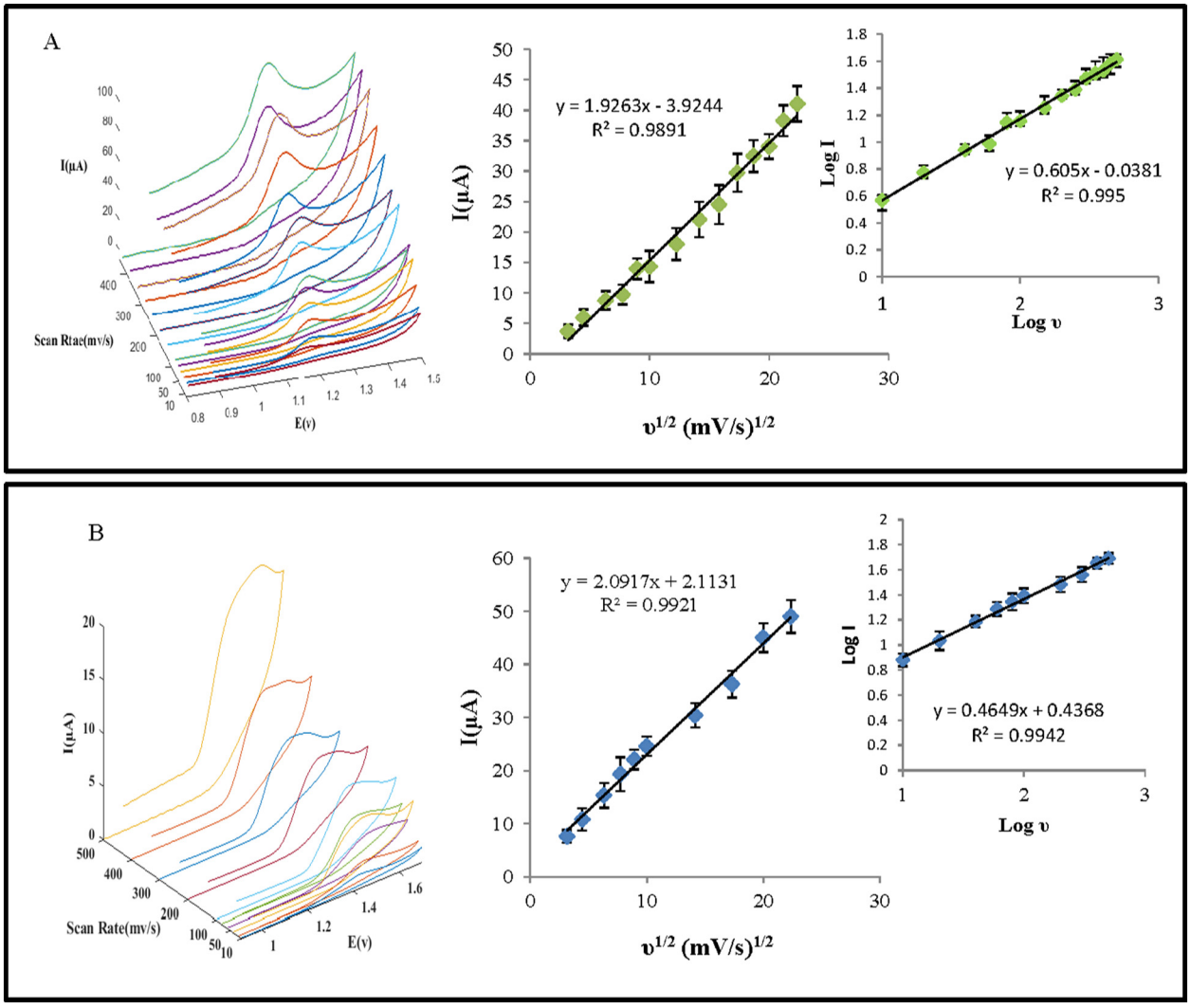

Fig. 5. CVs of A) 1.0 μM CA and B) 1.0 μM FEN in B-R buffer solution (pH = 3.0) at different scan rates using rGO/Cu/CuO-Ag/GCE, plots of peak current *vs.* $\upsilon^{1/2}$ and Log I *vs.* Log υ (inset).

concentration from 0.05 to 20 μM in the presence of 1.0 μM of FEN. Similarly, the oxidation peak currents of FEN increase linearly to the concentrations of the range of 0.01–30.0 μM while the concentration of CA (1.0 μM) remained constant (Fig. 6B). These results indicated that the measurement of CA and FEN in the mixture solution was not significantly interfered by the other compound. The linear regression equation of peak current and concentration of CA and FEN are as follows:

I_{pa} (CA) = 1.549C + 0.410 R^2 = 0.998

I_{pa} (FEN) = 2.420C + 0.685 R^2 = 0.997

The detection limits (DLs) of 5.0 and 3.0 nM were obtained for CA and FEN with rGO/Cu/CuO-Ag/GC, respectively.

The DPV responses of the rGO/Cu/CuO-Ag/GCE in the mixture of CA and FEN were examined while concentrations of two species were changed in the mixture. Fig. 6C showed the peak currents of CA and FEN increased with increasing their concentrations in the range of 0.05–20 and 0.01–30 μM, respectively. DLs were calculated 5.5 nM and 3.2 nM for CA and FEN, respectively. As shown in the Table 1, the detection limit and linear calibration range of the new sensor are comparable with and even in most cases better than values of DLs of separately pesticides and indicated that these species do not interfere with each other's determination with the low detection limit and broad linear range.

3.7. Reproducibility, repeatability and stability study of rGO/Cu/CuO-Ag/GCE

The response of rGO/Cu/CuO-Ag/GC in B-R solution containing 5.0 μM of CA and FEN was investigated to studied reproducibility. The five individual electrodes were prepared at similar conditions and the relative standard deviations (RSDs) less than 2.4% and 2.9% were obtained for CA and FEN, respectively.

To study the repeatability of the proposed sensor, the DPV responses of 5.0 μM of CA and FEN for 5 successive times were cheeked. The RSDs obtained for CA and FEN are 3.1% and 3.4% that the reproducibility of the electrode is acceptable. The stability of the designed sensor was also investigated when not used and it was kept in the laboratory for 5 days. The DPV signal for a mixture solution of CA and FEN (5.0 μM) was noted and compared with its response at the first day. According to the results, peak current had a small change (approx. 4%) and this shows its significantly stability.

3.8. Interference studies

The selectivity of the rGO/Cu/CuO-Ag/GCE toward CA and FEN were examined by different potentially interfering substance as

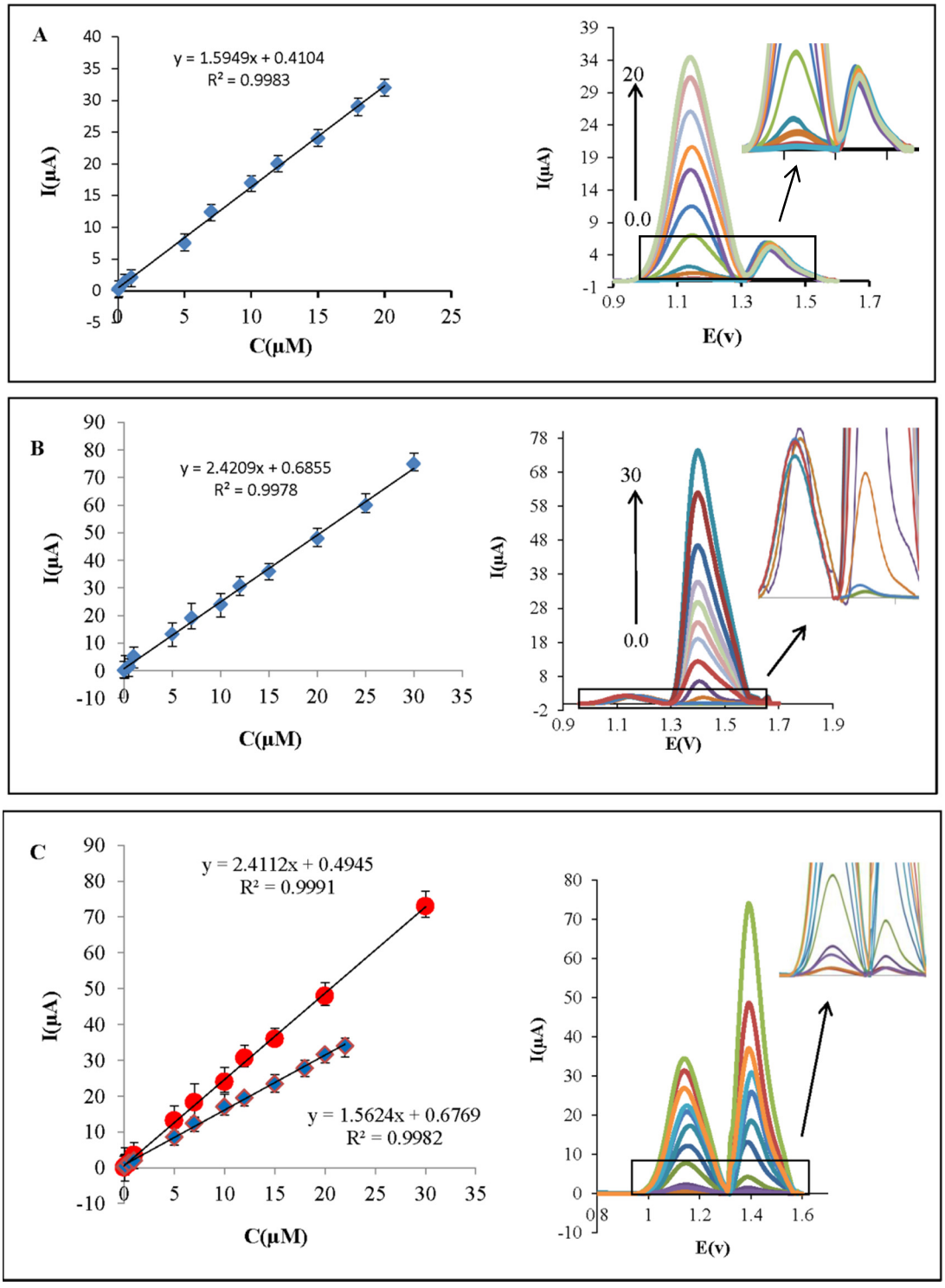

Fig. 6. DPVs of A) different concentrations of CA (0.05–20.0 μM) in the presence 1.0 μM FEN, B) different concentrations of FEN (0.01–30.0 μM) in the presence 1.0 μM CA at the rGO/Cu/CuO-Ag/GCE, C) different concentrations of 0.05 to 20.0 and 0.01 to 30.0 μM for CA, and FEN, in the B-R buffer solution (pH = 3.0), scan rate = 100 mV s^{-1}.

inorganic species and pesticides. The change of current responses of designed sensor was investigated in the various ratios between concentration of interference and analyte. The tolerance limit is defined as the concentration of the interfering component which causes an error of less than ± 5% in the determination of target analyte. The result showed that peaks signals of CA and FEN in the presence 1000 fold excess of Cl^-, SO_4^{2-}, CO_3^{2-}, NO_3^-, PO_4^{3-}, Cu^{2+}, Zn^{2+}, Pb^{2+}, Fe^{2+} and Cd^{2+} and 500 fold excess of phenol, quinone and bisphenol, have an error of less than ± 4%.

Also, pesticides such as parathion, diazinon, chlorpyrifos and paraoxan at 100-fold concentration excess in the presence of 1.0 μM CA and FEN, indicating no significant interferences on the detection of the target analytes (Fig. 7). Therefore, the fabricated sensor is suitable for the simultaneous determination of CA and FEN in the complex samples without separation.

Table 1
Comparison of the proposed sensor with the reported sensors for the determination of CA and FEN.

Method	Analyte	Electrode	LR (μM)	LOD (μM)	Reference
SWV	FEN	Boron-doped diamond	4.95–36.7	4.1	[11]
DPV	CA	CoO/rGO/GCE	0.5–200	0.037	[12]
SWV	CA	GC/MWCNT/CoPc film	0.33–6.61	0.005	[30]
SWV	FEN	BDD electrode	0.5–25.0	–	[31]
SWV	CA	GO-IL/GCE	0.10–12.0	0.02	[32]
SWV	CA	BDD	2.5–30.0	0.04	[33]
Chronoamperometry	CA	GC/MWCNT/PANI/AChE	–	1.4	[34]
Amperometry	CA	MWCNTs/GONR	0.005–5.0	0.017	[35]
DPV	CA	CP-SPE	0.1–1000	0.08	[36]
Amperometry	CA	AChE-CAMC/SPCE	0.049–2.4	0.0198	[37]
Cyclic voltammetry	CA	BDD	–	0.005	[38]
DPV	CA	ZXCPE	1.0–100.0	0.3	[39]
Cyclic voltammetry	CA	AChE-CHIT/Au	2.48–24.84	0.014	[40]
Chronoamperometry	CA	Au/PAMAM/GLUT/AChE	1.0–9.0	0.032	[41]
DPV	CA	3DG-Au/GCE	0.004–0.3	0.0012	[42]
SWV	FEN	GCE	0.5–25	0.1	[43]
DPV	CA	rGO/Cu/CuO-Ag/GCE	0.05–20.0	0.005	This work
DPV	FEN	rGO/Cu/CuO-Ag/GCE	0.01–30.0	0.003	This work

SWV: Square wave voltammetry, DPV: Differential pulse voltammetry, CV: cyclic voltammetry, BDD: boron-doped diamond, CoPc:cobalt phthalocyanine, MWCNTs/GONR: multiwall carbon nanotubes/graphene oxide nanoribbons, CP-SPE: carbon black- screen printed electrode, ZXCPE: zeolite X modified carbon paste electrode, AChE-CHIT: Acetylcholinesterase-chitosan, 3DG: three-dimensional graphene.

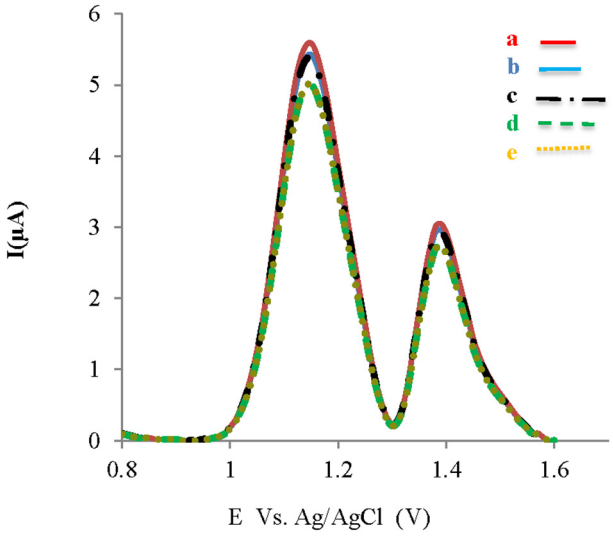

Fig. 7. DPVs of a) 1.0 μM of CA and FEN in B-R buffer solution (pH = 3.0) in the presence of b) parathion, c) Chlorpyrifos, d) diazinon, e) paraoxon.

Table 2
Simultaneous determination of CA and FEN in fruit and vegetable samples.

Sample	Added (μM)	Founded (μM)[a]	Recovery%	RSD%
Grape	1.0	1.05	105.0	2.1
	5.0	5.82	97.0	3.1
	10.0	15.7	98.1	4.2
Orange	1.0	0.98	98.0	1.9
	5.0	6.08	101.3	2.8
	10.0	16.51	103.1	3.4
Tomato	1.0	0.96	96.0	2.8
	5.0	6.21	103.5	3.6
	10.0	15.9	99.3	2.9
Cabbages	1.0	1.04	104.0	4.6
	5.0	6.34	105.6	3.8
	10.0	15.43	102.8	2.9

[a] Each value is the average of three determination.

3.9. Real samples

To assess the practical application, concentrations of CA and FEN using the rGO/Cu/CuO-Ag/GCE with the standard addition method were determined in the grape, orange, tomatoe and cabbage samples. Table 2 shows the data obtained with the proposed sensor are satisfactory, indicating the reliability of rGO/Cu/CuO-Ag/GCE for the determination of CA and FEN in the real samples.

4. Conclusion

It was possible to conclude from the results obtained that the GCE modified with rGO/Cu/CuO-Ag nanocomposite was used as a simple, inexpensive and highly sensitive electrochemical sensor for the determination pesticides of CA and FEN. The excellent sensing performance can be attributed to high surface area and excellent electrical conductivity of nanocomposite which leading to fast electron transfer rate. Fabricated sensor was also applied to detect two pesticides in different samples of vegetables and fruits. Recoveries were obtained between 96.0 and 105% for the analysis of CA and FEN that were acceptable.

Acknowledgement

The authors would like to thank National Institute for Medical Research Development (NIMAD) for the financial support this work (Grant No. 965379).

References

[1] G.S. Garbellini, G.R. Salazar-Banda, L.A. Avaca, Food Chem. 116 (2009) 1029–1035.
[2] S. Liu, Z. Zheng, X. Li, Anal. Bioanal. Chem. 405 (2013) 63–90.
[3] X. Guanggang, L. Diqiu, Y. Jianzhong, G. Jingmin, Z. Huifeng, S. Mingan, T. Liming, Food Chem. Toxicol. 53 (2013) 352–358.
[4] D. Bilehal, M. Chetti, G. Deepa, M. Khetagoudar, Analytical Chemistry Letters 6 (2016) 688–696.
[5] B. Cavaliere, M. Monteleone, A. Naccarato, G. Sindona, A. Tagarelli, J. Chromatogr. A 1257 (2012) 149–157.
[6] A.V. Veglia, Molecules 5 (2000) 437–438.
[7] C. March, J. Manclús, Y. Jiménez, A. Arnau, A. Montoya, Talanta 78 (2009) 827–833.
[8] T.M. Oliveira, M.F. Barroso, S. Morais, M. Araújo, C. Freire, P. de Lima-Neto, A.N. Correia, M.B. Oliveira, C. Delerue-Matos, Biosens. Bioelectron. 47 (2013) 292–299.
[9] S. Luo, Y. Wu, H. Gou, Ionics 19 (2013) 673–680.

[10] G. Liu, Y. Lin, Anal. Chem. 78 (2006) 835–843.
[11] T. Lima, H. Silva, G. Labuto, F. Simões, L. Codognoto, Electroanalysis 28 (2016) 817–822.
[12] M. Wang, J. Huang, M. Wang, D. Zhang, J. Chen, Food Chem. 151 (2014) 191–197.
[13] K. Justice Babu, S. Sheet, Y.S. Lee, G. Gnana kumar, ACS Sustain. Chem. Eng. 6 (2018) 1909–1918.
[14] K.D. Gilroy, A. Ruditskiy, H.-C. Peng, D. Qin, Y. Xia, Chem. Rev. 116 (2016) 10414–10472.
[15] Q. Kang, T. Wang, P. Li, L. Liu, K. Chang, M. Li, J. Ye, Angew. Chem. 127 (2015) 855–859.
[16] K.L. Klein, A.V. Melechko, P.D. Rack, J.D. Fowlkes, H. Meyer, M.L. Simpson, Carbon 43 (2005) 1857–1863.
[17] G. Jain, L. Patil, Sensors Actuators B Chem. 123 (2007) 246–253.
[18] S. Bennici, A. Gervasini, V. Ragaini, Ultrason. Sonochem. 10 (2003) 61–64.
[19] W. Vastarella, R. Nicastri, Talanta 66 (2005) 627–633.
[20] Z. Liu, R. Zhou, X. Zheng, J. Mol. Catal. A Chem. 267 (2007) 137–142.
[21] C.-Y. Huang, Y.-M. Sun, C.-Y. Chou, C.-C. Su, J. Power Sources 166 (2007) 450–457.
[22] A.K. Sasmal, S. Dutta, T. Pal, Dalton Trans. 45 (2016) 3139–3150.
[23] Y. Liang, Z. Chen, W. Yao, P. Wang, S. Yu, X. Wang, Langmuir 33 (2017) 7606–7614.
[24] K. Tian, C. Liu, H. Yang, X. Ren, Colloids Surf. A Physicochem. Eng. Asp. 397 (2012) 12–15.
[25] M. Srivastava, M.E. Uddin, J. Singh, N.H. Kim, J.H. Lee, J. Alloys Compd. 590 (2014) 266–276.
[26] F.T. Johra, J.-W. Lee, W.-G. Jung, J. Ind. Eng. Chem. 20 (2014) 2883–2887.
[27] A. Bonanni, A.H. Loo, M. Pumera, TrAC Trends Anal. Chem. 37 (2012) 12–21.
[28] H. Bagheri, A. Afkhami, H. Khoshsafar, M. Rezaei, A. Shirzadmehr, Sensors Actuators B Chem. 186 (2013) 451–460.
[29] E. Laviron, J. Electroanal. Chem. Interfacial Electrochem. 100 (1979) 263–270.
[30] F.C. Moraes, L.H. Mascaro, S.A. Machado, C.M. Brett, Talanta 79 (2009) 1406–1411.
[31] R.F. Franca, H.P.M. de Oliveira, V.A. Pedrosa, L. Codognoto, Diam. Relat. Mater. 27 (2012) 54–59.
[32] B. Liu, B. Xiao, L. Cui, J. Food Compos. Anal. 40 (2015) 14–18.
[33] L. Codognoto, S.T. Tanimoto, V.A. Pedrosa, H.B. Suffredini, S.A. Machado, L.A. Avaca, Electroanalysis: An International Journal Devoted to Fundamental and Practical Aspects of Electroanalysis 18 (2006) 253–258.
[34] I. Cesarino, F.C. Moraes, M.R. Lanza, S.A. Machado, Food Chem. 135 (2012) 873–879.
[35] Q. Liu, A. Fei, J. Huan, H. Mao, K. Wang, J. Electroanal. Chem. 740 (2015) 8–13.
[36] F. Della Pelle, C. Angelini, M. Sergi, M. Del Carlo, A. Pepe, D. Compagnone, Talanta 186 (2018) 389–396.
[37] J. Cai, D. Du, J. Appl. Electrochem. 38 (2008) 1217–1222.
[38] T.N. Rao, B. Loo, B. Sarada, C. Terashima, A. Fujishima, Anal. Chem. 74 (2002) 1578–1583.
[39] F.E. Salih, B. Achiou, M. Ouammou, J. Bennazha, A. Ouarzane, S.A. Younssi, M. El Rhazi, J. Adv. Res. 8 (2017) 669–676.
[40] D. Du, J. Ding, J. Cai, A. Zhang, Colloids Surf. B: Biointerfaces 58 (2007) 145–150.
[41] C.S. Santos, R. Mossanha, C.A. Pessôa, J. Appl. Electrochem. 45 (2015) 325–334.
[42] T. Rahmani, H. Bagheri, M. Behbahani, A. Hajian, A. Afkhami, Food Anal. Methods 11 (2018) 3005–3014.
[43] B. Qader, M.G. Baron, I. Hussain, R.P. Johnson, J. Gonzalez-Rodriguez, Monatshefte für Chemie-Chemical Monthly 150 (2019) 411–417.